SIMULATION-DRIVEN TOOLING SHAPE OPTIMIZATION FOR AN EASIER ASSEMBLING PROCESS OF COMPOSITE PARTS

B. Wucher[a*], F. Lani[b], T. Pardoen[b], C. Bailly[c], D. Dumas[a], P. Martiny[a]

[a] *Composite Structures and Processes, Cenaero, Rue des Frères Wright 29, 6041 Gosselies, Belgium*
[b] *Institute of Mechanics, Materials and Civil Engineering, Université catholique de Louvain, Place Sainte Barbe 2, 1348 Louvain-la-Neuve, Belgium*
[c] *Institute of Condensed Matter and Nanosciences, Université catholique de Louvain, Croix du Sud 1, 1348 Louvain-la-Neuve, Belgium*
**benoit.wucher@cenaero.be*

Keywords: Cure, Shape distortions, Shape optimization, Assembling.

Abstract
The respect of the manufacturing tolerances is a challenging issue due to the complex distortions caused by the curing process, being sometimes a major obstacle to an increasing use of composites in aeronautics. In this study, a generic tooling shape optimization strategy is developed and tested on a curved CFRP C-spar. Finite element curing simulations enable to assess the cure-induced distortions. Included in an optimization loop with an innovative parametrization strategy, they allow for the alteration of the mold shape in order to reduce the discrepancy between the original design and the produced composite part.

1. Introduction

Typical epoxy-based composite materials show significant distortions as a consequence of the manufacturing process. These distortions lead to deviations with respect to the manufacturing tolerances and to assembling difficulties. The physical origin for the distortion is a combination of several phenomena, of which the most important are the chemical shrinkage, the mismatch of coefficient of thermal expansion (CTE) between the fibers and the matrix, and the partly irreversible thermal expansion of the resin due to the significant CTE variations during the cure. Cure-induced distortions are most commonly observed as spring-in or warpage of the composite part after removal from the mold. Two main approaches can be investigated to reduce the discrepancy between the nominal geometry and the final part. A first option is to improve the manufacturing process. Teoh and Hsiao [1] observed a spring-in reduction of L-shaped parts by using the multistage curing technique and the Vacuum Assisted Resin Transfer Molding process. Hsiao and Gangireddy [2] proposed to include carbon nanofibers in a polyester resin in order to reduce the anisotropy of the thermal expansion of the material and, hence, reduce the spring-in. Jain et al. [3] optimized experimentally the spring-in of a thermoplastic C-shaped aileron rib by changing the cure temperature. Jung et al. [4] predicted the distortions of U- and C-shaped composite parts, but performed the compensation only experimentally. A second option consists in using numerical simulations to guide towards an optimal shape of the mold so that the final part is as close as possible to the nominal geometry. This approach is called “mold compensation”, and is the subject of the present work. Dong [5] developed a simplified curing model, created

designs of experiments for several basic composite structures with only a few parameters and developed a regression-based spring-in reduction method. Dong [6] studied the effect of the curing process on a parametrized stiffener without including the model in an optimization loop. Zhu and Geubelle [7] used an optimizer to alter the mold shape for L-shaped parts. All the aforementioned methods have been tested only on L-shaped-like composite parts, which can easily be broken down to a one-parameter mono-objective optimization. Fernlund and Floyd [8] developed process modeling capabilities and applied them to tool compensation involving several distortion modes of curved L-angles [9] but the compensation strategy was solely based on analytical considerations. Through the PRECIMOULD project, cure modeling was implemented in the commercial software Lusas [10]. Although mold compensation was an objective of the project, very little information can be found about the underlying methodology. Therefore, the literature does not yet provide a systematic distortion compensation strategy for complex geometries. This contribution presents an attempt to fill this gap. A full optimization chain is developed, including CAD parametrization, automatic draping simulation and a 3D computationally-efficient chemical-mechanical curing model. This chain is then used in an in-house surrogate-based optimizer, MINAMO [11], to modify the geometry of the mold and to minimize the mismatch between the nominal and actual shape of the part after demolding. The combination of automatic draping and surrogate models allows to imagine the application of this technique to virtually any geometry. A moderately complex geometry is tested in this work, namely a curved CFRP C-spar. A novel shape optimization technique is presented. Instead of parametrizing the part with angles to compensate for spring-in, a certain number of points are chosen on the geometry. The position of those points is parametrized, so that they can move freely in space to ultimately find the optimal mold configuration.

2. Test case

2.1 Geometry

The chosen test case is a generic curved C-spar, as shown in Fig. 1. It was modeled as a surface because it is easier to create the CAD model and much easier to drape compared to a volume model. This geometry was selected because it is simple enough to provide a first demonstration test case, and complex enough to enforce the need for a draping simulation. The dimensions are 440 mm in curvilinear length, 100 mm in width and 55 mm in height. The fillet radius along the length of the C-spar is 8.5 mm. The C-spar is curved and forms an arc of a circle with a radius of 450 mm.

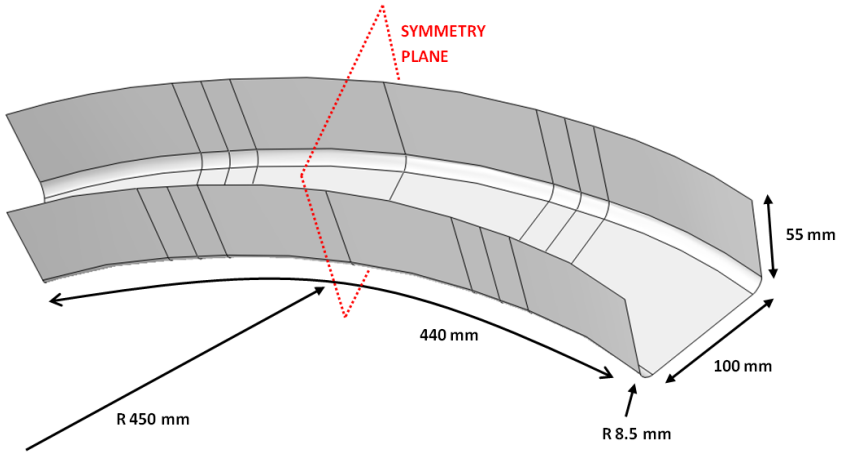

Figure 1. Surface geometry of the curved C-spar.

2.2 Material

For this proof of concept, the C-spar was manufactured with a low-temperature resin (Huntsman's Araldite LY5052 and hardener Aradur HY5052 at a ratio of 100:38), with 5-harness satin carbon fibers by Porcher (370 g/m²). Five C-spars were manufactured by the VARTM process with four plies of the carbon textile, and the thickness was measured at 1.85 mm, which implies a fiber volume fraction of 46 %. The properties for the simulations were determined from micromechanics considerations, based on typical properties for carbon fibers (Table 1 [12,13]) and the resin properties given by Svanberg (Table 2 [14]). The results of these calculations are given in Table 3. The degree of cure at gelation is equal to 0.5 [15]. The relationships between the degree of cure X and the glass transition temperature, and the kinetic model are given by Eq. 1, and Eqs. 2 and 3, respectively [16], with T being the temperature, and R being the universal gas constant.

$$T_g(°C) = 128 - 250 * (1 - X) \quad , \tag{1}$$

$$\frac{dX}{dt}(s^{-1}) = 110000\, e^{\frac{-52600}{RT(K)}} X^{0.17} (X_{max} - X)^{1.83} \quad , \tag{2}$$

$$X_{max} = 0.782 + 0.002 * T(°C) \quad . \tag{3}$$

3. Setup of the computational chain

3.1 Parametrization

A novel parametrization technique is set up in this work: instead of parametrizing the part with angles to compensate for spring-in, a certain number of points are chosen on the geometry. The position of those points is parametrized, so that they can move freely in space to ultimately find the optimal mold configuration. This allows the optimizer to test very complex configurations that could not be obtained by anticipation from the designer. This technique can be adapted to virtually any geometry, the only thinking process being the choice of the control points. It does not require to anticipate the cure-induced distortions of the part, to the contrary of classical compensation techniques (opening of angles to suppress spring-in, etc...). For the present test case, the chosen control points are displayed in Figure 2. An example of deformed geometry is given in Figure 3. The fact that the part is symmetric allows for a complete description of its surface by only 12 points. Each point has 3 degrees of freedom, which leads to 29 parameters after suppressing the rigid body motions.

Property	Value
E_L	230 GPa [12]
E_T	14 GPa [12]
ν_{LT}	0.2 [12]
ν_{TT}	0.25 [12]
G_{LT}	9 GPa [12]
α_L	-6.10^{-7} /°C [13]
α_T	15.10^{-6} /°C [13]

Table 1. Typical properties of carbon fibers. Subscripts L and T stand for the longitudinal and transverse directions, respectively. α is the coefficient of thermal expansion (CTE).

Property	Rubbery state	Glassy state
E	2.8 MPa	2.6 GPa
ν	0.499	0.38
α	178.10^{-6} /°C	71.10^{-6} /°C
β	-0.023	-0.023

Table 2. Mechanical properties of LY5052/HY5052 epoxy resin system [14]. β is the chemical shrinkage coefficient.

Property	Rubbery state	Glassy state
$E_1 = E_2$	52.9 GPa	56.7 GPa
E_3	8.7 MPa	5.8 GPa
ν_{12}	0.36	0.3
$\nu_{23} = \nu_{13}$	0.52	0.36
G_{12}	2.9 MPa	2.4 GPa
$G_{23} = G_{13}$	2.9 MPa	2.5 GPa
$\alpha_1 = \alpha_2$	$-5.8.10^{-7}$ /°C	$4.2.10^{-6}$ /°C
α_3	3.10^{-4} /°C	$1.2.10^{-4}$ /°C
$\beta_1 = \beta_2$	$-2.5.10^{-6}$	-0.0018
β_3	-0.038	-0.034

Table 3. Mechanical properties of carbon 5-H satin/LY5052 system during cure, determined by micromechanics considerations. Subscripts 1 and 2 stand for the in-plane directions, 3 is the transverse direction.

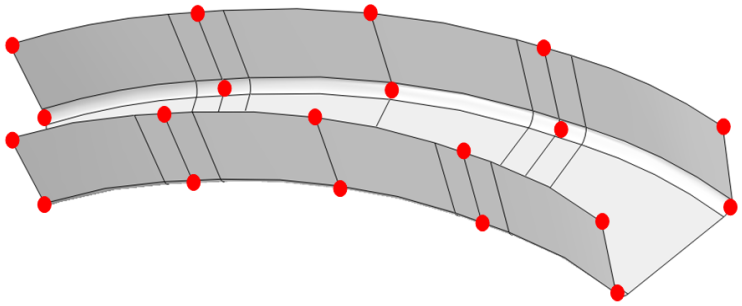

Figure 2. Red dots are the chosen control points for the parametrization of the geometry

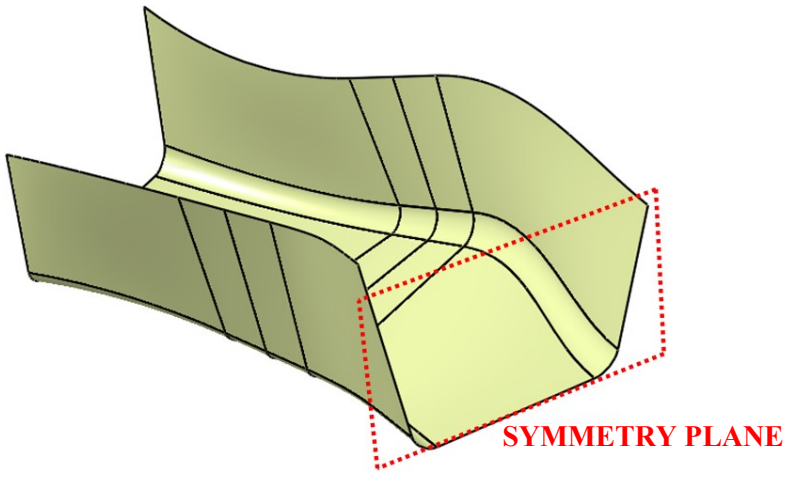

Figure 3. An exaggerated example of the shape that the parametrized mold can take during the optimization

3.2 Prediction of the cure-induced distortions

Running an optimization implies automating the link between the compensated geometry and the prediction of its cure-induced distortions. The computational chain takes the deformed CAD as input. This surface is draped with Simulayt [17]. The plies are draped in such a way that the warp direction of the satin fabric follows the curvature of the part. Then, a volume mesh with the proper orientations is obtained thanks to an in-house extrusion tool.

Since the curing simulation is included within an optimization loop, it must be as computationally efficient as possible. For this reason, it is assumed that the temperature is uniform throughout the part. This is a valid hypothesis (the C-spar is 1.85 mm thick), and it limits the analysis to a mechanical-chemical problem only, instead of a transient coupled thermo-mechanical-chemical one. Moreover, the simulation takes advantage of the symmetry of the geometry, which further reduces the computational time.

The mechanical model used in this study for curing is the one developed by Svanberg and Holmberg [15]. The main assumptions include the fact that no stresses build up before the gel point, that the material properties are constant within each state of the material (rubbery or glassy), and that chemical shrinkage and thermal expansion are linear, with a change of slope at vitrification. The applied cure cycle is shown in Figure 4. The cure and post-cure cycles were designed, based on the T_g and kinetics models (Eqs. (1) and (2)), to reach a high level of cure and to stay in the glassy state during post-cure. The cycle is as follows : heat-up from 20°C to 60°C with a ramp of 2°C/min, a 10-hour hold at 60°C, cool-down to 20°C at 3°C/min, then a slow heating ramp of 0.15°C/min to reach the post-cure temperature of 100°C, with a subsequent hold of 10 hours. Final cool-down ramp is 3°C/min as well. The predicted final degree of cure is 98 %. The time step is set equal to 300 seconds, which is small enough to capture the correct evolution of the degree of cure, and large enough to enable an efficient computation time. Freestanding boundary conditions are used, i.e. only rigid body modes are suppressed and the mold itself is not modeled. The validity of this assumption largely depends on the actual manufacturing process, particularly the friction between the composite part and the mold can play a role. However, in this work, we do not focus on the accuracy of the curing model, but on the mold compensation technique.

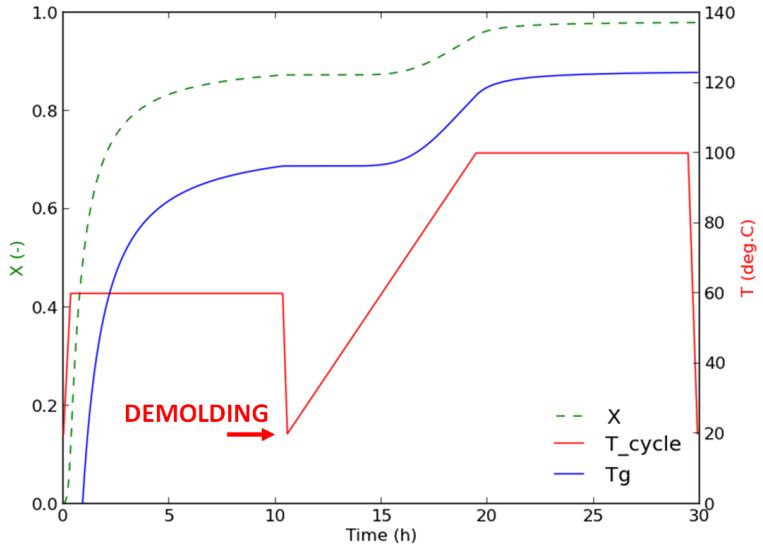

Figure 4. Cure and post-cure cycles. Tg and X are not measured but computed thanks to numerical models of Eqs. (1) and (2), respectively.

The duration of the curing simulation on the C-spar (78,000 degrees of freedom) is equal to 8 minutes on six cores of a double hexa-core Intel Xeon (3.07 GHz) computation node. The analysis necessitates about 2.5 GB of RAM and is performed with Abaqus/Standard through a user material (UMAT) for the implementation of the constitutive law.

3.3 Evaluation of the cure-induced distortions

A post-processing step is added after the curing simulation, to compute the cure-induced distortions. Figure 5 represents the displacement field of the cured nominal geometry. Several definitions of the distortions can be made (spring-in, warpage, …), but in the interest of keeping a generic compensation technique, the distortions are here defined as the distance between the control points after cure and their position on the nominal geometry. To that end, a best-fit is performed, and the distance between the nominal and cured geometries is taken as the sum of the residual distances at the control points. This is summarized by Figure 6. The purpose of the optimization is then to reduce the residual distance D_{min}.

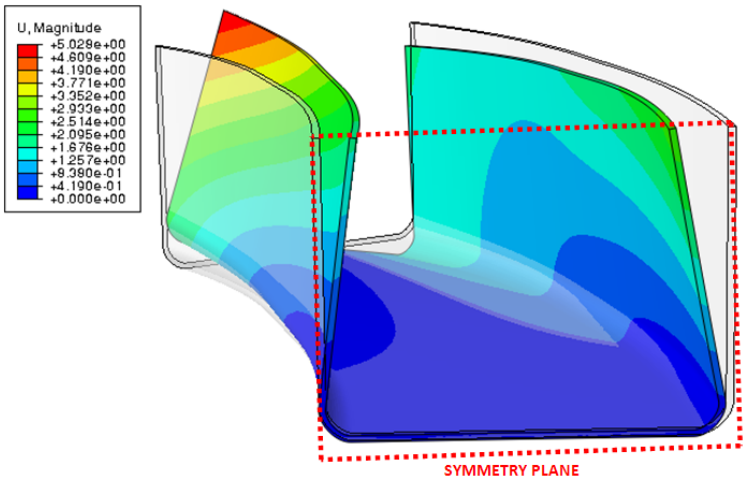

Figure 5. Displacement field after cure of the nominal geometry (deformation factor: 5). Torsion and spring-in can be clearly observed.

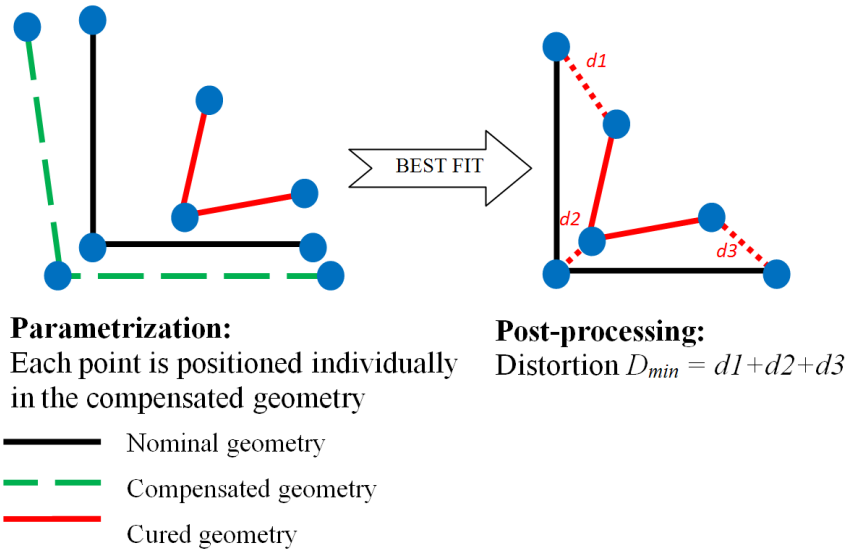

Figure 6. Illustration of how the cure-induced distortions are evaluated

4. Optimization results

The optimizer MINAMO can perform Surrogate-based Optimizations (SBO), where the design space is sampled and a surface is fitted through the sampled points. Then the optimizer finds the optimum of the surface and uses this result to improve its quality. More information can be found in [11]. This approach is particularly efficient with a high number of parameters, which is the case here (29 parameters).

Figure 7 presents the convergence history of the optimization. The distance D_{min} is normalized by its nominal value. The final value of the normalized distance is 0.169, which means that the residual distance was reduced by 83.1 % over the course of the optimization. Starting from a value of 31.2 mm (2.6 mm per control point on average), the residual distance was reduced to 5.3 mm (0.44 mm per point on average).

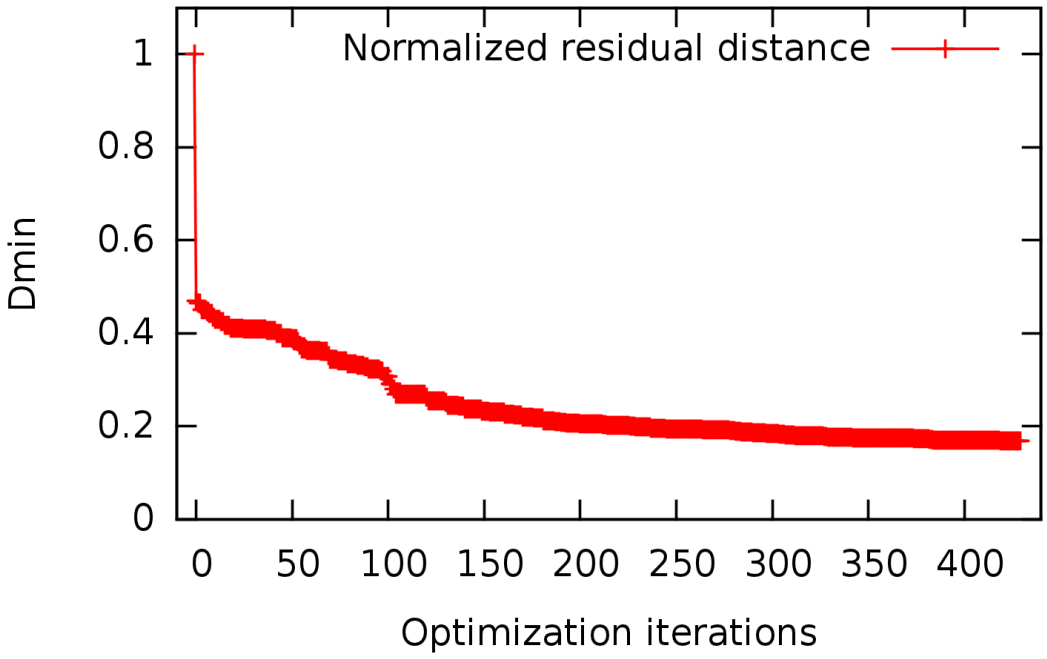

Figure 7. Optimization convergence

5. Experimental validation

An attempt of experimental validation has been made. The objective was to compare the measured distortions with the numerically-predicted distortions, on the nominal geometry. However, the variability proved to be too high to be able to draw any conclusions. The principal causes for this variability is the use of VARTM as manufacturing process, which is hardly repeatable in a satisfactory manner. This will be further investigated in the coming months.

6. Conclusion

A computational chain designed to compensate for cure-induced distortions was presented in this work. Several tools were developed to benefit from the high-fidelity draping on a surface model as well as from 3D curing simulations. An innovative parametrization was proposed, whose principle does not depend on the studied geometry and is therefore readily applicable to other geometries. The optimizer managed to reduce by 83 % the distance criterion, ending

up with a residual distance of 0.44 mm per control point. This method hereby provides a generic method to help designers alter the shape of their molds to reduce the discrepancy between the original design and the produced composite part. An additional ambition of this work was to perform a low-cost experimental validation of the distortion values of the initial geometry, but the time frame and insufficient experimental capabilities did not enable to produce satisfactory results.

References

[1] K. J. Teoh and K. T. Hsiao. Improved dimensional infidelity of curve-shaped VARTM composite laminates using a multi-stage curing technique – Experiments and modeling. *Composites : Part A*, 42:762-771, 2011.

[2] K. T. Hsiao and S. Gangireddy. Investigation on the spring-in phenomenon of carbon nanofiber-glass fiber/polyester composites manufactured with vacuum assisted resin transfer molding. *Composites : Part A*, 39:834-842 2008.

[3] L. Jain, M. Hou, L. Ye, Y. W. Mai. Spring-in study of the aileron rib manufactured from advanced thermoplastic composite. *Composites : Part A*, 29A:973-979, 1998.

[4] W. K. Jung, B. Kim, M. S. Won, S. H. Ahn. Fabrication of radar absorbing structure (RAS) using GFR-nano composite and spring-back compensation of hybrid composite RAS shells. *Composite Structures*, 75:571-576, 2006.

[5] C. Dong. Dimension variation prediction and control for composites. Thesis. Florida State University, 2003.

[6] C. Dong. Process-induced deformation of composite T-stiffener structures. *Composite Structures*, 92:1614-1619, 2010.

[7] Q. Zhu and P. Geubelle. Dimensional accuracy of thermoset composites : shape optimization. *Journal of Composite Materials*, 36:647-672, 2002.

[8] G. Fernlund, A. Osooly, A. Poursartip, R. Vaziri, R. Courdji, K. Nelson, P. George, L. Hendrickson, J. Griffith. Finite element based prediction of process-induced deformation of autoclaved composite structures using 2D process analysis and 3D structural analysis. *Composite Structures*, 62:223-234, 2003.

[9] G. Fernlund, A. Floyd. Process analysis and tool compensation for curved composite L-angles. In: Proceedings of *The Sixth Canadian-International Composites Conference*, 2007.

[10] T. Garstka, G. Cole, D. Irving, P. Lyons. Integrated finite element environment for composite process simulation. In: Proceedings of *ICCM17: International Conference on Composite Materials*, 2009.

[11] C. Sainvitu, V. Iliopoulou, I. Lepot. Global optimization with expensive functions – sample turbomachinery design application. In Springer, *Recent Advances in Optimization and its Applications in Engineering*, pages 499-509, 2010.

[12] F. Stig and S. Hallström. Spatial modelling of 3D-woven textiles. *Composite Structures*, 94:1495-1502, 2012.

[13] G. Korb, J. Koráb, G. Groboth. Thermal expansion behaviour of unidirectional carbon-fibre-reinforced copper-matrix composites. *Composites : Part A*, 29A:1563-1567, 1998.

[14] J. M. Svanberg and J. A. Holmberg. Prediction of shape distortions. Part II. Experimental validation and analysis of boundary conditions. *Composites : Part A*, 35:723- 734, 2004.

[15] J. M. Svanberg and J. A. Holmberg. Prediction of shape distortions. Part I. FE-implementation of a path dependent constitutive model. *Composites : Part A,* 35:711-721, 2004.

[16] J. M. Svanberg. Shape distortion of non-isothermally cured composite angle bracket. *Plastics Rubber and Composites,* 31:398-404, 2002.

[17] Simulayt software package, www.simulayt.com.